Journal of Sol-Gel Science and Technology (2018) 85:647–656
https://doi.org/10.1007/s10971-017-4568-8

ORIGINAL PAPER: SOL-GEL AND HYBRID MATERIALS FOR CATALYTIC, PHOTOELECTROCHEMICAL AND SENSOR APPLICATIONS

Selective catalytic reduction of NO_x by CO over $LaMnO_3$ nano perovskites prepared by microwave and ultrasound assisted sol–gel method

Seyed Ali Hosseini[1] · Behrouz Mehri[1] · Aligholi Niaei[2] · Behrang Izadkhah[2] · Consuelo Alvarez-Galvan[3] · Jose G. Luis Fierro[3]

Received: 9 October 2017 / Accepted: 19 December 2017 / Published online: 5 February 2018

Abstract

A series of $LaMnO_3$ perovskites as catalysts for selective reduction of NO by CO were synthesized using microwave and ultrasound assisted sol-gel method. The catalysts were characterized by BET area measurements, Scanning Electron Microscopy (SEM), X-Ray diffraction (XRD) and X-ray Photoelectron Spectroscopy (XPS) techniques. XRD results showed revealed the orthorhobic crystalline structure and with very high purity. SEM analyses proved lower particle size for ultrasound (US) assisted synthesized $LaMnO_3$. In addition, US assisted synthesized $LaMnO_3$ presented higher surface area respect to other catalysts, synthesized by the other methods. Results revealed that the ultrasound assisted synthesized catalyst determines the lowest crystallite size, the highest surface area and the highest concentration of O-vacancies and, as a consequence, the highest catalytic activity.

Graphical Abstract

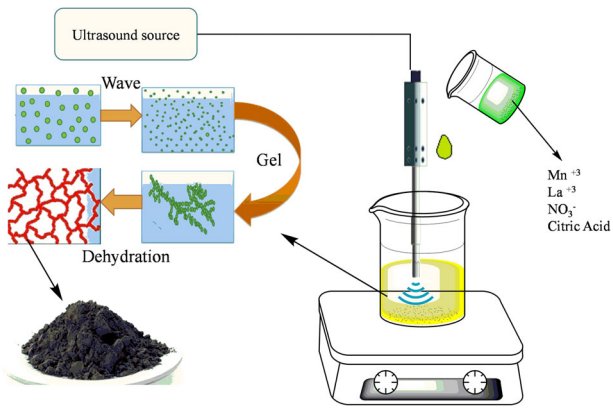

Keywords NO reduction · Nano Perovskite · Microwave · Ultrasonic · Sol-gel

✉ Seyed Ali Hosseini
a.hosseini@urmia.ac.ir

[1] Department of Applied Chemistry, Faculty of Chemistry, Urmia University, Urmia, Iran

[2] Catalyst & Reactor Research Group, Department of Chemical and Petroleum Engineering, University of Tabriz, Tabriz, Iran

[3] Instituto de Catálisis y Petroleoquímica CSIC Cantoblanco E-28049 Madrid, Spain

1 Introduction

The emission of nitrogen oxides (NO_x) and carbon monoxide (CO) is an important problem from environmental and public health point of view [1]. NO_x and CO are believed to have important role in global warming, acid rain and photochemical smog formation [2]. The oxidation of CO is not only of interest to eliminate this poisonous compound from exhaust, but also can be utilized as a test reaction for structure–activity correlation studies [3]. Many catalysts [4–6] have been investigated and used in the CO oxidation reactions. Among them, noble metal catalysts (e.g., Au) are capable of full CO conversion even at ambient reaction temperature, but they are susceptible to sintering and are expensive, and furthermore, their activity decreases by increasing the reaction time [4]. Perovskite oxides are excellent candidates as catalysts, particularly suited for exhaust gas depollution processes. They can be regarded as valuable catalysts, alternative to supported noble metals since they are easily synthesized at lower cost and with increased thermal stability up to high temperatures [7–9]. These solids have a well-defined crystalline structure represented by the general formula ABO_3, where A designates a cation of rare earth, alkaline earth, alkali or ions with a large ionic radius, like Pb^{2+} or Bi^{3+} and B a transition metal cation from the groups 3d, 4d or 5d [10–12]. Their catalytic properties have been extensively studied for oxidation and reduction reactions. However, the low specific surface areas of perovskites (<10 m^2/g) prepared by conventional synthesis routes, limit their efficiency in catalytic processes [13, 14]. In the last decades, great efforts to obtain perovskites with increased specific surface area have been carried out. For example, Nandi and co-workers reported the synthesis of high surface area $LaMnO_3$ by hydrothermal method using saturated fatty acids as templates in the presence of ethylenediamine (EDA) as mineralizer [15]. Micro emulsion synthesis and supported perovskite synthesis are examples of attempts in order to enhance the surface area of perovskite catalysts [16–19]. However, mentioned methods are not efficient enough because of introduction of inert or poisonous materials. Recently, there have been several attempts to synthesize supported metal catalysts with improved particle dispersion using microwave-assisted or ultrasonic wave-assisted techniques [20, 21]. The use of ultrasound (US) irradiation in chemistry has grown significantly, resulting in a considerable part of empirical research. In this technique, the reactant molecules undergo chemical reactions due to the application of powerful US waves (20 kHz–1 MHz) [22, 23]. It is considered as a 'green' technology owing to its high efficiency, low instrumental requirements, significantly reduced process time compared with other conventional techniques and its economically viable performance [24, 25]. The sonochemical process in liquids is based on the generation, growth, and collapse of bubbles, also known as acoustic cavitation, which results in extreme local heating, high pressures, and very short lifetimes [26, 27]. As a result, many chemical reactions that were previously difficult to carry out by other heating methods, can easily be accomplished using sonication [28]. Similar to other chemical processes, utilization of US in synthesis of perovskite oxide has many advantages including an increase in specific surface area, improved metal dispersion and, as a result, enhanced catalytic performances [29]. In addition, utilization of US in perovskite oxide synthesis can lead to a reduction in crystallite size of final compound [24, 27, 29]. Another alternative to conventional methods is utilization of microwave (MW) irradiation, which is an effective method to improve chemical processes. MW radiation is the term associated with any electromagnetic radiation in the microwave frequency range of 300 MHz–300 GHz [30, 31]. In many cases, MW assisted chemical reactions have displayed spectacular accelerations and/or higher yields under milder reaction conditions [32–34]. Utilization of MW in synthesis of perovskite oxides has many advantages such as higher structural defects, reduced crystallite size [35], etc.

The aim of this research is to utilize MS and MW in order to improve the catalytic performance of $LaMnO_3$ perovskite. Thus, $LaMnO_3$ perovskite catalysts have been synthesized using US, MW, US-MW assisted and conventional sol–gel autocombustion methods in different experimental conditions, and tested in CO oxidation and simultaneous NO + CO removal reactions. In particular, this research will focus on the preparation of $LaMnO_3$ perovskites with higher surface area. To correlate the physico-chemical properties of synthesized catalysts (resulting from the preparation method) with the catalytic performance; the characterizations will be carried out using adsorption–desorption of N_2 at −196 °C (BET surface area), Scanning Electron Microscopy (SEM), X-Ray diffraction (XRD) and X-ray Photoelectron Spectroscopy (XPS) techniques.

2 Experimental section

2.1 Catalysts preparation

The $LaMnO_3$ perovskite were prepared by four methods: conventional sol−gel autocombustion, US, MW, and US-MW assisted solgel autocombustion.

2.1.1 Sol–gel method

Appropriate amounts of $La(NO_3)_3{\cdot}6H_2O$ and $Mn(NO_3)_2{\cdot}3H_2O$ were dissolved in a certain amount of distilled water

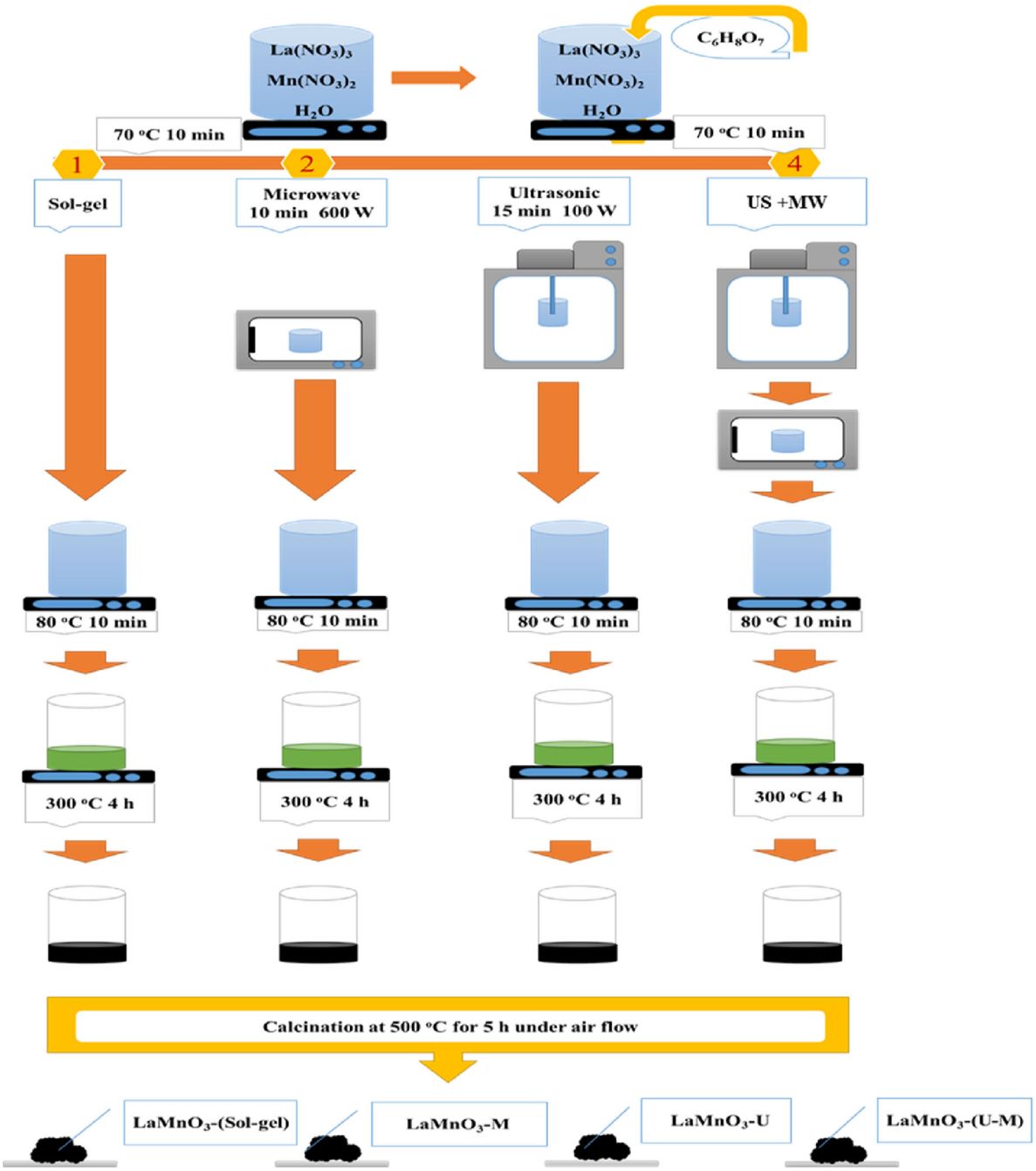

Fig. 1 Preparation steps of nanostructured $LaMnO_3$ catalyst with different methods

with a continuous stirring. The resulting solution was heated at 70 °C for 10 min, and then, a given amount of citric acid (Merck) was added to the solution, using a molar ratio of citric acid to the total amount of nitrates in the solution mixture of 0.525 [36]. After, the resulting solution was heated at 80 °C for 10 min and it gradually turned into a sticky gel. The wet gel was charred at 300 °C in air for 4 h to remove the organic compounds and the nitrates, being obtained a dark powder which was finally calcined at 500 °C for 5 h in static air.

The US and MW treatments have been used before the evaporation step.

2.1.2 US assisted method

The US treatment has been performed using a Sonicator with a frequency of 20 kHz, an effective input power of 100 W (determined by a calorimetric calibration) and a tip diameter of 13 mm. The solution of La and Mn nitrates and

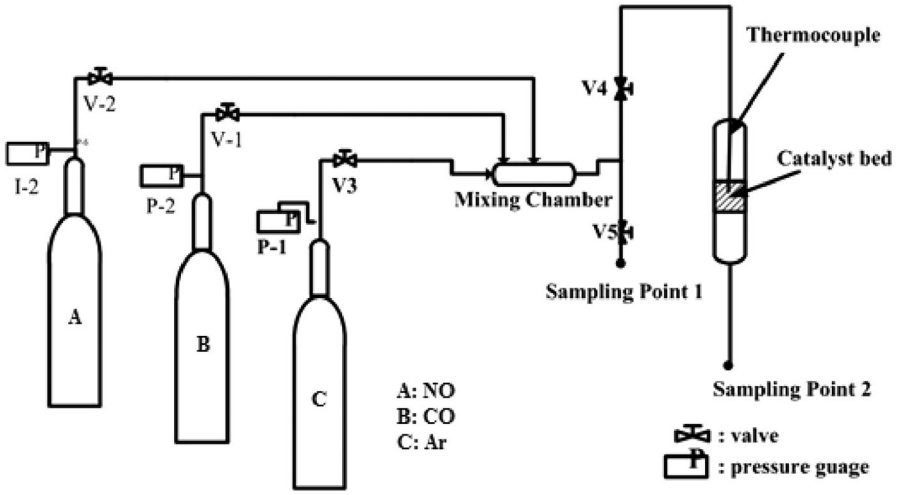

Fig. 2 Experimental setup NO + CO reaction

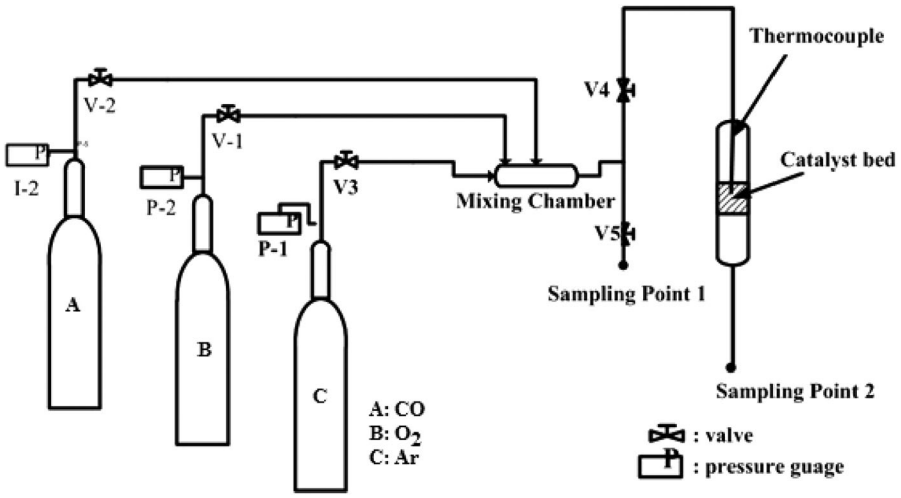

Fig. 3 Experimental setup for CO Oxidation reaction

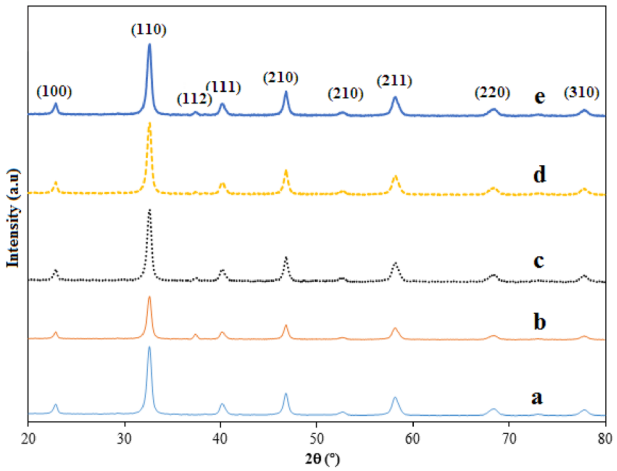

Fig. 4 XRD patterns of the catalysts: **a** reference LaMnO3 (JCPDS 01-075-0440), **b** sol–gel, **c** MW, **d** US, **e** MW + US

citric acid have been sonicated by the US horn for 15 min under air atmosphere.

Table 1 Crystallite size and BET surface area of synthesized catalysts

Compound	Crystallite size (nm)	Surface area (m^2/g)
$LaMnO_3$—sol–gel	48	27.4
$LaMnO_3$—MW	39	33.8
$LaMnO_3$—US	31	36.3
$LaMnO_3$—MW-US	34	34.7

2.1.3 MW assisted method

The MW treatment has been performed in air atmosphere using an oven powered at 600 W for 10 min. Temperature was at 30 °C by an external air cooling flow.

2.1.4 US and MW assisted method

A combination of US and MW was also utilized for $LaMnO_3$ synthesis. The combination has been carried out

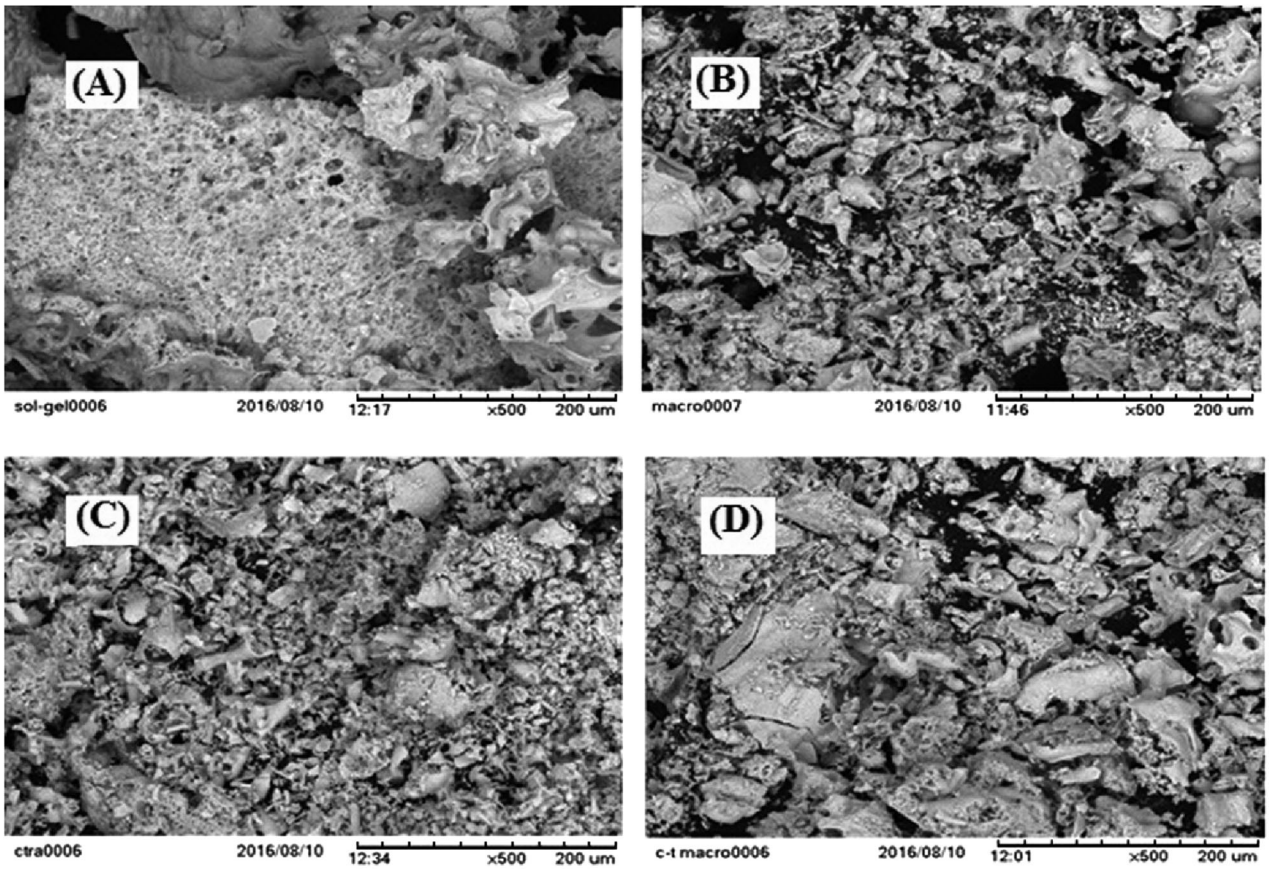

Fig. 5 SEM images of nano-sized $LaMnO_3$ catalysts: **a** $LaMnO_3$-(sol–gel), **b** $LaMnO_3$-MW, **c** $LaMnO_3$-US and **d** $LaMnO_3$-(US-MW)

by utilization of US (15 min, 100 W) prior to MW (10 min, 600 W) before the evaportion step.

A simple scheme of catalyst preparation routes is shown in Fig. 1.

2.2 Characterization techniques

Different techniques including XRD, SEM, XPS, and BET were applied to characterize the synthesized catalysts. The phase structures of the nanostructured catalysts were appraised utilizing a Siemens D500 diffractometer (Germany) and Cu K_α radiation ($\lambda = 1.54$ Å). Diffractograms were recorded with a step of 4° per minute for 2θ between 20 and 80°. JCPDS files were employed for phase identification. Mean size of crystallites (D) were calculated by means of the Scherrer equation $D = K\lambda/(\beta \cos\theta)$. In this equation, K is a constant value equal to 0.89, λ is the wavelength of the used X-ray and β is the effective line width of the X-ray reflection. Surface areas were calculated from the N_2 isotherms recorded at −196 °C using a micropore analyzer (ASAP 2010, USA) and taking a value of 0.162 nm^2 for the cross section of adsorbed N_2 molecule. The morphology of the synthesized catalysts at a micrometric-scale was determined by SEM (Hitachi TM-1000). The surface elemental composition and oxidation state of the atoms at the surface were examined by XPS, using a VG ESCALAB spectrometer provided with AlKα X-ray source and hemispherical electron analyzer. The C 1s peak at 284.8 eV, corresponding to the signal for adventitious carbon was used as an internal standard for peak position correction.

2.3 Experimental setup for catalytic performance test

Figures 2 and 3 illustrates the experimental setup employed to evaluate the catalyst performance. The schematic diagram consists of a gas feeding section, a fixed bed reactor and an analytical section. The NO + CO reaction was performed over a temperature range of 100 to 500 °C at atmospheric pressure using 0.2 g catalyst in a fixed-bed quartz reactor (8 mm internal diameter). The reactant gases were NO (99.999%—Technical Gas Service), and CO (99.999%—Technical Gas Service) and argon as balance gas. In addition, feed ratio was NO:CO = 1:1 in all the experiments. The reactor effluent line was connected to a

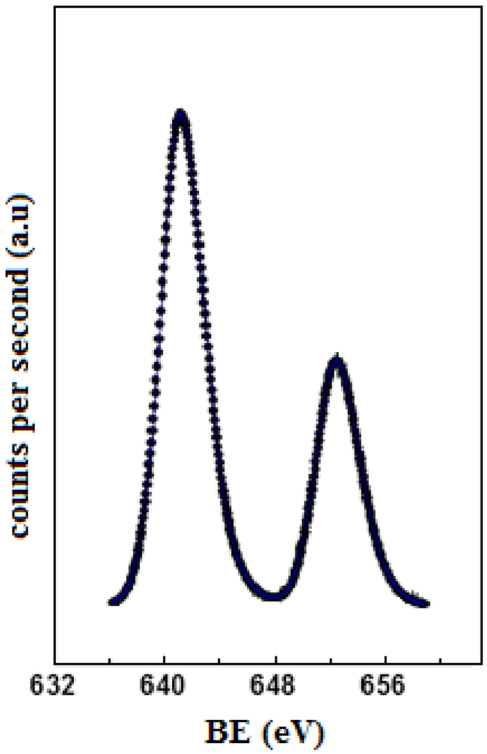

Fig. 6 Mn 2p core level spectra of different catalysts

GC gas-sampling valve to analyze the products. Besides, the CO oxidation reaction was performed over a temperature range from 70 to 230 °C at atmospheric pressure using 0.2 g catalyst in a fixed-bed quartz reactor (8 mm i.d.). The reactant gases were CO (99.999%- Technical Gas Service), oxygen (99.999%—Technical Gas Service) and argon as the balance gas.

3 Results and discussion

The XRD patterns of catalysts are presented in Fig. 4. All the catalysts displayed the orthorhombic crystal structure of $LaMnO_3$ (JCPDS ICDD file No. 01-075-0440). All diffraction lines were indexed to the orthorhombic crystal system except for the weak peak at 2θ around 37° which is assigned to MnO_2. This last phase is scarcely formed in the sample prepared by US treatment. As mentioned above, the average crystallite size of $LaMnO_3$ was evaluated by the Scherrer equation, and results are collected in Table 1. Based on the results from Table 1, the US assisted synthesis method resulted in the lowest cristallite size, being the trend for $LaMnO_3$ cristallite size is as follows:

$$LaMnO_3 - sol - gel > LaMnO_3 - MW > LaMnO_3 - MW - US > LaMnO_3 - US$$

Figure 5 shows the SEM images of lanthanum manganite-based nanocatalysts synthesized using various methods. As it is shown in Fig. 4, the sonochemical method had higher effect on decreasing particle size of catalysts. In other word, the SEM images show that the US assisted synthesis method had higher ability to prevent particles agglomeration respect to sol–gel, MW and US-MW methods. Thus, it appears that the repulsive force decreased the particles propensity to agglomerate. Surface areas of the catalysts, which are reported in third column of Table 1, show that the US assisted synthesis results in the highest surface area. This observation is in agreement with the results of crystallite size measurements and SEM images and in accordance with the fact that for these bulk materials the only contribution to surface area is the geometric surface area of the particles. Indeed, the lower crystallite size and the lower particle size lead to higher surface area. The order found for the surface area is:

$$LaMnO_3 - US > LaMnO_3 - MW - US > LaMnO_3 - MW > LaMnO_3 - sol - gel$$

Surface analysis was carried out for all these catalysts using XPS. The Mn2p and O1s core level spectra, are presented in Figs. 6 and 7, respectively. The Mn2p of the all catalysts was the same as presented in Fig. 6. The binding energy of Mn2p is in agreement with the presence of Mn^{3+} in $LaMnO_3$. O 1s spectra showed two peaks, centered on 529 and 531 eV, in all catalysts. The low binding energy peak is assigned to lattice oxygen, while the high binding energy one can be related with adsorbed carbonate or surface hydroxyl groups. The binding energies (reported in Table 2) is typical of La^{3+} in an $LaMnO_3$ (or La_2O_3) structure [37, 38].

Table 2 also shows atomic surface ratios, which indicate that these values are close to the nominal bulk ones, with a slight enrichment of the surface by lanthanum species. Concerning the ratio surface oxygen species to lattice oxygen, the sample prepared by MW treatment presents the highest value. Figure 8 shows the catalytic performance of the synthesized catalysts for the reduction of NO with CO. As it is expected, NO and CO conversion increased by increasing the reaction temperature. The 50% NO conversion temperature for $LaMnO_3$-(sol–gel), $LaMnO_3$-MW, $LaMnO_3$-(US-MW) and $LaMnO_3$-US were 330, 310, 270, and 215 °C, respectively. Besides, 50% conversion temperature of CO for $LaMnO_3$-(sol–gel), $LaMnO_3$-MW, $LaMnO_3$-(US-MW) and $LaMnO_3$-US were 365, 335, 300, and 235 °C, respectively. The order of catalytic activity for NO + CO reaction is: $LaMnO_3$-US > $LaMnO_3$-US-MW > $LaMnO_3$-MW > $LaMnO_3$-(sol–gel). So, it resulted that US assisted synthesized $LaMnO_3$ is the most active catalyst

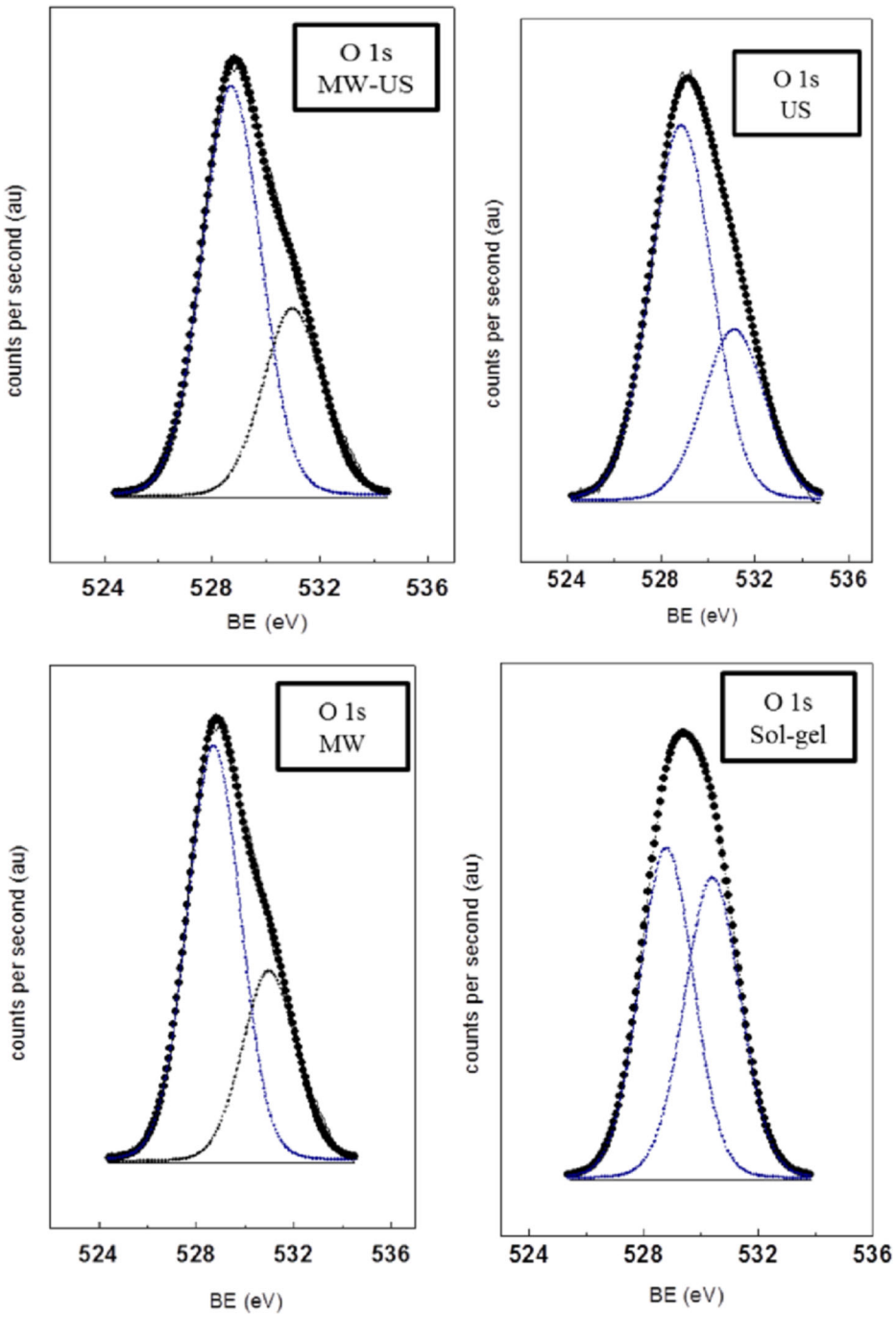

Fig. 7 O 1s core level spectra of different catalysts

among the different $LaMnO_3$. There are two main nitrogen containing products for NO + CO reaction including N_2 and N_2O. Figure 9 shows temperature profiles for the yield of N_2O over the catalysts. Production of N_2O starts at low temperatures and reaches a maximum at about 300 °C depending on the composition of the sample and at higher temperatures its formation decreases.

Figure 10 shows the catalytic performance of the synthesized catalysts for CO Oxidation. The temperature corresponding to 80% of carbon monoxide conversion for $LaMnO_3$-(sol–gel), $LaMnO_3$-MW, $LaMnO_3$-(US-MW), and $LaMnO_3$-US were 225, 210, 190, and 150 °C, respectively. Therefore, the order found for catalytic activity in CO oxidation is: $LaMnO_3$-US > $LaMnO_3$-US-MW > $LaMnO_3$-MW > $LaMnO_3$-(sol–gel).

Therefore, the order found for the catalytic activity of synthesized catalysts in both CO + NO and CO oxidation reactions was: $LaMnO_3$-US > $LaMnO_3$-US-MW > $LaMnO_3$-MW > $LaMnO_3$-(sol–gel). The higher activity for $LaMnO_3$-US is influenced by the lower crystallite size.

Table 2 Binding energy (eV) of core-levels and atomic ratios of lanthanum manganites samples

Sample	$La3d_{5/2}$	$Mn2p_{3/2}$	O1s	C1s	Mn/La	CO_3^{2-}/La
MW			528.9 (60)			
	834.0	641.5	530.7 (40)	288.4	0.925	0.411
MW + US			528.8 (68)			
	833.9	641.4	531.0 (32)	288.3	0.824	0.592
sol–gel			528.8 (67)			
	834.0	641.4	531.0 (33)	288.2	0.977	0.334
US			528.9 (69)			
	834.0	641.5	531.0 (31)	288.3	0.943	0.355

Peak percentages in parentheses

CO_3^{2-}/La is the concentration of carbonate structures developed on the sample surface

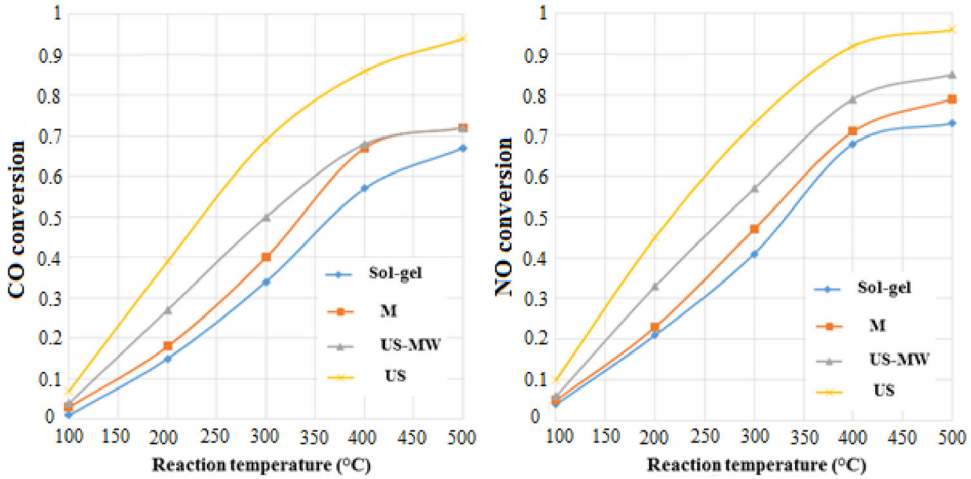

Fig. 8 NO and CO Conversions versus reaction temperature for NO + CO reaction

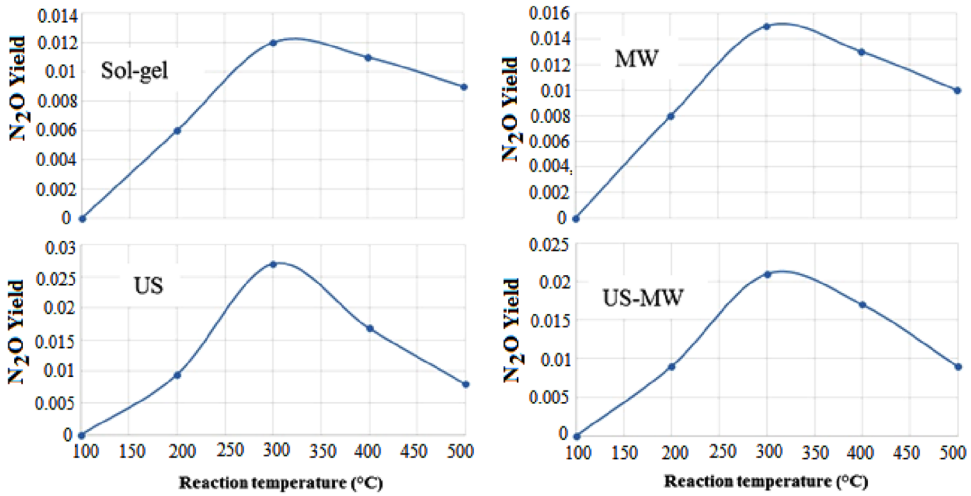

Fig. 9 N_2O yield versus reaction temperature for NO + CO reaction

Actually, as it was previously commented, lower crystallite size was related to higher surface area and lower particle size. The worst catalytic performance displayed by the catalyst prepared by the sol–gel method is explained, not only by its lowest surface area and greater crystalline domain (or crystallite size), but also the greatest formation of MnO_2, as it was observed in the corresponding X-ray diffractogram.

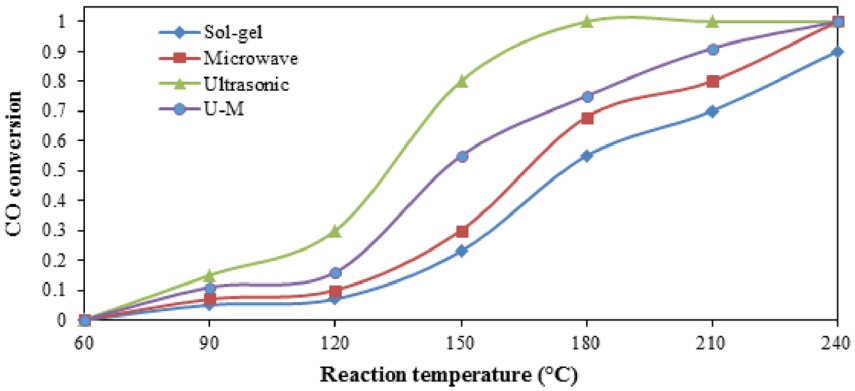

Fig. 10 CO Conversion versus reaction temperature for CO + O_2 reaction

4 Conclusions

The $LaMnO_3$ perovskite catalysts were succesfully synthesized using MW and US assisted sol–gel method as well as conventional sol–gel method. XRD results showed that all the catalysts display the characteristic orthorhobic crystalline structure and with very high purity. In addition, based on this technique, the mean crystallite size revealed that the US assisted synthesized $LaMnO_3$ has the lowest crystallite size (31 nm). At the micrometric level, SEM analyses proved lower particle size for US assisted synthesized $LaMnO_3$. In addition, US assisted synthesized $LaMnO_3$ presented higher surface area respect to other catalysts, synthesized by the other methods. Therefore, lower crystallite size and higher surface area could result in higher surface oxygen vacancies which would result in higher catalytic performance as it was observed for US assisted $LaMnO_3$ catalysts in CO + NO reaction and CO oxidation reaction. Accordingly, the US assisted method has been assessed as a useful tool in the preparation of perovskite catalysts because of many favorable features, which were achieved for the synthesis of $LaMnO_3$ catalyst.

Acknowledgements We especially thank Iranian Nanotechnology Initiative Council for financial supports.

Compliance with ethical standards

Conflict of interest The authors declare that they have no conflict of interest.

References

1. Khristova M, Petrović S, Terlecki-Baričević A, Mehandjiev D (2009) Catalytic reduction of NO by CO over Pd—doped Perovskite-type catalysts. Open Chem 7:857–863
2. Wang Y, Zhu A, Zhang Y, Au C, Yang X, Shi C (2008) Catalytic reduction of NO by CO over NiO/CeO_2 catalyst in stoichiometric NO/CO and NO/CO/O_2 reaction. Appl Catal B 81:141–149
3. Ciambelli P, Cimino S, Lasorella G, Lisi L, De Rossi S, Faticanti M, Minelli G, Porta P (2002) CO oxidation and methane combustion on $LaAl_{1-x}Fe_xO_3$ perovskite solid solutions. Appl Catal B 37:231–241
4. Lian H, Jia M, Pan W, Li Y, Zhang W, Jiang D (2005) Gold-base catalysts supported on carbonate for low-temperature CO oxidation. Catal Commun 6:47–51
5. Royer S, Duprez D (2011) Catalytic oxidation of carbon monoxide over transition metal oxides. ChemCatChem 3:24–65
6. Allian AD, Takanabe K, Fujdala KL, Hao X, Truex TJ, Cai J, Buda C, Neurock M, Iglesia E (2011) Chemisorption of CO and mechanism of CO oxidation on supported platinum nanoclusters. J Am Chem Soc 133:4498–4517
7. Daly F, Schmitt J, Sturm E (1986) Molybdenum-support interaction and its effect on nitric oxide chemisorption and temperature-programmed desorption. J Catal 97:248–251
8. Mizuno N, Misono M (1998) Heterogeneous catalysis. Chem Rev 98:199–218
9. Pena M, Fierro J (2001) Chemical structures and performance of perovskite oxides. Chem Rev 101:1981–2018
10. Tejuca LG, Fierro J (2000) Properties and applications of perovskite-type oxides. CRC Press, New York
11. Russo U, Nodari L, Faticanti M, Kuncser V, Filoti G (2005) Local interactions and electronic phenomena in substituted $LaFeO_3$ perovskites. Solid State Ion 176:97–102
12. Bernard C, Dauzet G, Mathieu F, Durand B, Puech-Costes E (2005) Optimization of the hydrothermal synthesis of $La_{0.7}Sr_{0.3}MnO_{3+\delta}$ using an original optimal experimental design. Mater Lett 59:2615–2620
13. Teraoka Y, Nii H, Kagawa S, Jansson K, Nygren M (2005) Influence of the simultaneous substitution of Cu and Ru in the perovskite-type (La, Sr) MO_3 (M = Al, Mn, Fe, Co) on the catalytic activity for CO oxidation and CO–NO reactions. Appl Catal A 194:35–41
14. Giannakas A, Leontiou A, Ladavos A, Pomonis P (2006) Characterization and catalytic investigation of NO + CO reaction on perovskites of the general formula $La_x M_{1-x} FeO_3$ (M = Sr and/or Ce) prepared via a reverse micelles microemulsion route. Appl Catal A 309:254–262
15. Nandi M, Sarkar K, Seikh M, Bhaumik A (2011) Mesoporous lanthanum–manganese oxides with nanoscale periodicity, high surface area and ferromagnetic property. Micro Mesopor Mater 143:392–397
16. Shi D, Hu R, Zhou Q, Yang L (2016) Catalytic activities of supported perovskite promoter catalysts La_2NiMnO_6–$CuCl_2$/γ-Al_2O_3 and $La_{1.7}K_{0.3}NiMnO_6$–$CuCl_2$/γ-Al_2O_3 for ethane oxychlorination. Chem Eng J 288:588–595
17. Giannakas AE, Ladavos AK, Pomonis PJ (2004) Preparation, characterization and investigation of catalytic activity for NO + CO reaction of $LaMnO_3$ and $LaFeO_3$ perovskites prepared via microemulsion method. Appl Catal B 49:147–158

18. Aman D, Zaki T, Mikhail S, Selim S (2011) Synthesis of a perovskite $LaNiO_3$ nanocatalyst at a low temperature using single reverse microemulsion. Catal Today 164:209–213
19. Giroir-Fendler A, Alves-Fortunato M, Richard M, Wang C, Díaz JA, Gil S, Zhang C, Can F, Bion N, Guo Y (2016) Synthesis of oxide supported $LaMnO_3$ perovskites to enhance yields in toluene combustion. Appl Catal B 180:29–37
20. Tsuji M, Hashimoto M, Nishizawa Y, Kubokawa M, Tsuji T (2005) Microwave-assisted synthesis of metallic nanostructures in solution. Chem Eur J 11:440–452
21. Suslick KS (1990) Sonochemistry. Science 247:1439–1445
22. Mason T, Lorimer J (2002) Applied sonochemistry: Uses of power ultrasound in chemistry. Wiley-VCH verlag GmbH, Weinheim
23. Suslick KS, Hammerton DA, Cline RE (1986) Sonochemical hot spot. J Am Chem Soc 108:5641–5642
24. Suslick K, Fang M, Hyeon T, Mdleleni M (1999) Applications of sonochemistry to materials synthesis. In: Crum LA et al. (eds) Sonochemistry and sonoluminescence, Springer, New York, pp 291–320
25. Mohideen MI, Allan PK, Chapman KW, Hriljac JA, Morris RE (2014) Ultrasound-driven preparation and pair distribution function-assisted structure solution of a copper-based layered coordination polymer. Dalton Trans 43:10438–10442
26. Suslick KS, Hyeon T, Fang M (1996) Nanostructured materials generated by high-intensity ultrasound: sonochemical synthesis and catalytic studies. Chem Mater 8:2172–2179
27. Suslick K, Doktycz S (1990) Effect of ultrasound on surfaces and solids. Adv Sonochem 1:197–230
28. Ahluwalia V, Kidwai M (2004) Ultrasound assisted green synthesis. In: Javed Iqbal (ed) New trends in green chemistry. Springer, New York, NY
29. Bang JH, Suslick KS (2010) Applications of ultrasound to the synthesis of nanostructured materials. Adv Mater 22:1039–1059
30. Ayas N, Yilmaz O (2015) Catalytic esterification and transesterification reaction of high acidic value waste oil by microwave heating. Environ Prog Sustain Energy 34:575–581
31. Kingman S (2006) Recent developments in microwave processing of minerals. Int Mater Rev 51:1–12
32. Zhang H, Ding J, Zhao Z (2012) Microwave assisted esterification of acidified oil from waste cooking oil by CERP/PES catalytic membrane for biodiesel production. Bioresour Technol 123:72–77
33. Azcan N, Danisman A (2008) Microwave assisted transesterification of rapeseed oil. Fuel 87:1781–1788
34. Hernando J, Leton P, Matia MP, Novella J, Alvarez-Builla J (2007) Biodiesel and FAME synthesis assisted by microwaves: homogeneous batch and flow processes. Fuel 86:1641–1644
35. Prado-Gonjal J, Gutiérrez-Seijas J, Ansorregui IH, Morán E, Terry I, Schmidt R (2016) The role of defects in microwave and conventionally synthesized $LaCoO_3$ perovskite. J Eur Ceram Soc 36:1197–1206
36. Arefi Oskoui S, Niaei A, Tseng HH, Salari D, Izadkhah B, Hosseini SA (2013) Modeling preparation condition and composition–activity relationship of perovskite-type $La_xSr_{1-x}Fe_yCo_{1-y}O_3$ nano catalyst. ACS Comb Sci 15:609–621
37. Alifanti M, Kirchnerova J, Delmon B (2003) Effect of substitution by cerium on the activity of LaMnO3 perovskite in methane combustion. Appl Catal A 245:231–243
38. Celorrio V, Calvillo L, Dann E, Granozzi G, Aguadero A, Kramer D, Russell AE, Fermín DJ (2016) Oxygen reduction reaction at $La_xCa1_{-x}MnO3$ nanostructures: interplay between A-site segregation and B-site valency. Catal Sci Technol 6:7231–7238